The Importance of Steric Influences in the Construction of Multi-component Hybrid Polymetallic Clusters

Ross McLellan,[†] Maria A. Palacios,[§] Sergio Sanz,[§] Euan K. Brechin[§]* and Scott J. Dalgarno[†]*

† Institute of Chemical Sciences, School of Engineering and Physical Sciences, Heriot-Watt University, Riccarton, Edinburgh, EH14 4AS, Scotland

§ EaStCHEM School of Chemistry, University of Edinburgh, David Brewster Road, Edinburgh, EH9 3FJ, Scotland

ABSTRACT: The straightforward room temperature synthesis of hybrid polymetallic manganese clusters is investigated, exploiting complementary ligand combinations of *p*-tert-butylcalix[4]arene and salicylaldoximes. Eight new [$Mn^{III}_7Mn^{II}$] clusters have been prepared wherein the simple substitution of alkyl or aryl groups at well-defined positions of the salicylaldoxime scaffold leads to two distinct structure types that, while exhibiting the same general topology, contain the unique Mn^{II} ion in different positions. Incorporation of a methyl, ethyl or isopropyl group at the 3-position of the aromatic skeleton or a phenyl group at the oximic carbon gives structure type A that displays competing weak ferromagnetic and antiferromagnetic interactions. Substitution of a methyl or ethyl group at the oximic carbon atom invokes structure type B, incorporating an additional bulky chloride or nitrate into the metallic core due to the smaller steric imposition and position of the methyl or ethyl group. The distortion of the cluster core is consequently enhanced, switching the magnetic properties and resulting in single-molecule magnet behavior. The presence of tert-butyl groups at the 3- and 5-positions of the salicylaldoxime skeleton leads to a new [$Mn^{IV}_2Mn^{III}_2$] cluster that is found to be a single-molecule magnet. The bulky tert-butyl group in the 3-position is too large to facilitate Mn_8 cluster formation, and thus assembly occurs by an alternative pathway. Characteristic bonding modes of the constituent ligands are retained in every case, and the results presented here give insight into the potential of ligand combinations in future studies, highlighting the importance of steric factors in evaluating their relevant compatibilities.

INTRODUCTION

For many years the field concerning the synthesis and study of polynuclear transition metal clusters has undergone rapid growth. This may be attributed in part to the relationship between the fascinating physical properties and potential low temperature applications that the molecules possess,[1] and the myriad of structures that they can adopt. Of the transition elements, perhaps the most intensely studied for cluster formation is manganese, for which initial interest stemmed from the oxygen evolving complex of photosystem II, which plays a crucial role in photosynthesis.[2] Subsequently, systematic studies in the application of polynuclear manganese compounds as nanoscale magnetic materials led to a further resurgence in research activity. As such, the structure of the first manganese single-molecule magnet (SMM) was reported by Lis in 1980.[3] This archetypal dodecanuclear [$Mn^{III}_8Mn^{IV}_4$] carboxylate cluster possesses a ground state spin (S = 10) and, importantly, large easy-axis anisotropy (highlighting the importance of Mn^{III} ions in SMMs), which enables the Mn_{12} complex to function as a SMM.[4] Although the Mn_{12} species remain benchmark compounds, the area has progressed significantly to include a plethora of SMMs of varying structure, nuclearity and with different oxidation state distributions. Structural effects are also important however, a fact that is perhaps best illustrated in a series of compounds constructed with phenolic oximes.[5] Using the salicylaldoxime family of ligands ($SaoH_2$, Figure 1A) a library of complexes based upon [Mn^{III}_3O]$^+$ building blocks (Mn^{III}_3 and Mn^{III}_6) revealed the magneto-structural relationship describing the effect of changing structural parameters (determined by the oximic R group modulating the pairwise exchange through manipulation of the Mn-O-N-Mn torsion angle) upon magnetic properties.[5]

A major challenge in this area is controlling the structure (and hence properties) of polymetallic clusters. Since serendipity is one of the main driving forces for cluster formation it is crucial that we understand the various coordination modes of the ligands involved. Knowledge of these, obtained through a thorough examination of the myriad of known compounds, can then give the synthetic chemist, at least in part, a degree of control over the likely molecular structure. For example, the aforementioned Sao^{2-} ligands tend to bond so as to bridge two metal ions, and the arrangement of donor atoms is such that the formation of species based upon Mn^{III}_3 triangles is favored (Figure 1B).

We have recently been exploring the coordination chemistry of the closely related *p-tert*-butylcalix[*n*]arenes (TBC[*n*]) and calix[*n*]arenes (C[*n*]s, Fig. 1C). C[*n*]s are cyclic polyphenolic macrocycles that adopt well defined and relatively rigid conformations as a consequence of hydrogen bonding interactions between phenolic hydroxyl groups at what is termed the lower-rim.[6] In an expanding body of work we (and others) have demonstrated that TBC[4] or C[4] readily coordinate a transition or lanthanide metal ion in the center of the polyphenolic cavity, with subsequent retention of the cone conformation.[7] Important breakthroughs in this regard include a [$Mn^{III}_2Mn^{II}_2$(TBC[4])$_2$] SMM (Fig. 1D),[7b,c] [$Mn^{III}_4Ln^{III}_4$(C[4])$_4$] (where Ln = Gd, Tb or Dy) clusters that are magnetic refrigerants or SMMs depending on the lanthanide employed (Fig. 1E),[7d,e] and a ferromagnetically coupled [Mn_5] cluster,

$[Mn^{III}_3Mn^{II}_2(TBC[4])_2(hmp)_2]$ (hmp = 2-(hydroxymethyl)pyridine).[7h] The latter was synthesized using complementary ligands that each display well-defined coordination motifs as shown in Figure 1F.

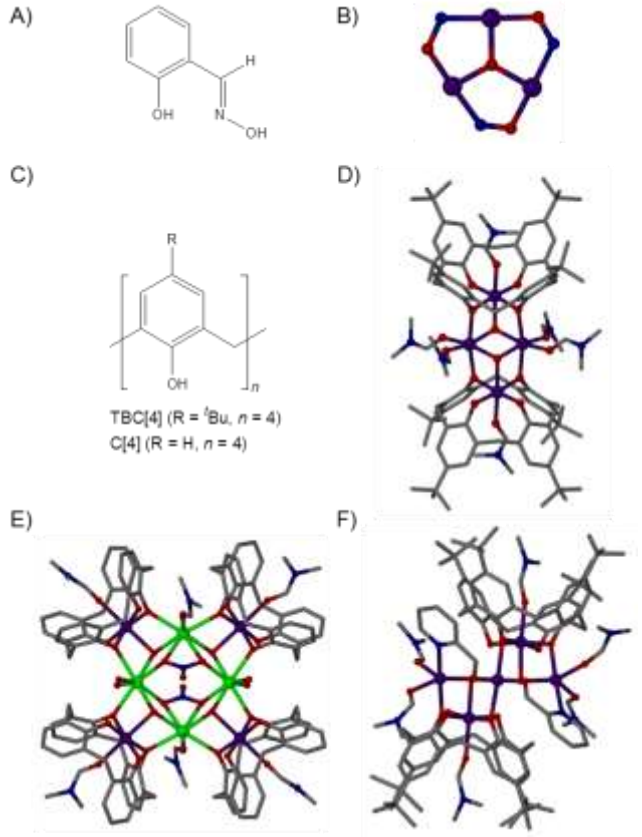

Figure 1. A) Schematic of the general salicylaldoxime ($SaoH_2$) skeleton. B) General triangular $[Mn^{III}_3O(N\text{-}O)_3]^+$ subunit resulting from the assembly of Mn^{III} ions and Sao^{2-} ligands.[5] C) Schematic of TBC[4] and C[4]. D) Structure of a $[Mn^{III}_2Mn^{II}_2(TBC[4])_2]$ SMM.[7b,c] E) Structure of $[Mn^{III}_4Ln^{III}_4(C[4])_4]$ magnetic refrigerant (Ln = Gd) or SMMs (Ln = Tb, Dy).[7d,e] F) Structure of ferromagnetic $[Mn^{III}_3Mn^{II}_2(TBC[4])_2(hmp)_2]$ cluster.[7h] Color code: C grey; O red; N blue; Mn purple; Ln green.

From the expanding library of clusters, we have established empirical metal-ion binding rules for these C[4] ligands. Of particular relevance here is the fact that the polyphenolic cavity has high affinity for Mn^{III} ions, which bind preferentially over TM^{II} or Ln^{III}.[7d,e,i] Thus the $[Mn^{III}TBC[4]]^-$ moiety can be considered a stable and persistent building block for cluster formation / structural fragment incorporation. By extension, it is likely that the combination of a wide-ranging array of competing or complementary ligands with TBC[4] will lead to new clusters with diverse topologies and properties depending on the co-ligand employed. Moreover, these new clusters should form with a degree of control in terms of the metal-ion binding properties, with the *proviso* that the binding properties of the co-ligand employed have been surveyed thoroughly.

RESULTS AND DISCUSSION

In this contribution we present our initial investigations into cluster formation using TBC[4] as a ligand support in combination with a series of $SaoH_2$ co-ligands; previously we noted that the combination of manganese with $PhSaoH_2$ and TBC[8] results in formation of a ferromagnetically coupled $[Mn^{IV}Mn^{III}]$ metal dimer supported by both ligands.[8] The general $SaoH_2$ skeleton can be readily altered at various positions via the formal substitution of either aromatic or oximic hydrogen atoms for simple aliphatic or aromatic substituents. We selected and synthesized ten candidates for our studies into cluster formation as shown in Figure 2.[9] From our experiments we found that reaction of **IV** – **VII** and TBC[4] with a source of Mn^{II} ions, in presence of base under ambient conditions, resulted in the formation of four new $Mn^{III}_7Mn^{II}$ clusters, **1-4**, all of which are supported by two tetra-anionic TBC[4] and three di-anionic Sao^{2-} ligands. The general structure can be described as a buckled $Mn^{III}_5Mn^{II}$ plane that is capped on each face by a $[Mn^{III}TBC[4]]^-$ moiety. The analogous reaction with **II** or **III** also results in formation of $Mn^{III}_7Mn^{II}$ clusters, **5-8**, however the central $Mn^{III}_5Mn^{II}$ plane exhibits markedly different coordination chemistry. The reaction of **X** under similar conditions resulted in the formation of a novel $[Mn^{IV}_2Mn^{III}_2]$ cluster containing no calixarene. From these studies we propose that the steric bulk presented by the tertiary butyl groups in **X** is too great to allow formation of a Mn_8 cluster. Reactions involving the remaining ligands **I**, **VIII** or **IX** in combination with TBC[4] and a source of Mn^{II} resulted in formation of the familiar $[Mn^{III}_2Mn^{II}_2(TBC[4])_2]$ cluster (Fig. 1D) as the only isolable product, suggesting that co-ligands may require particular structural features that offer a degree of cooperativity in cluster formation with TBC[4]; groups positioned around the $SaoH_2$ that are either too small or too large may be unfavorable for cluster formation due to a) their inability to form complementary interactions with TBC[4] or b) steric properties that render them incompatible co-ligands.

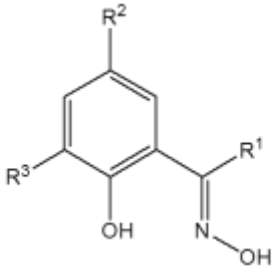

	R^1	R^2	R^3		R^1	R^2	R^3
I	H	H	H	**VI**	H	H	Et
II	Me	H	H	**VII**	H	H	Me
III	Et	H	H	**VIII**	H	tBu	H
IV	Ph	H	H	**IX**	H	H	tBu
V	H	H	iPr	**X**	H	tBu	tBu

Figure 2. Ten $SaoH_2$-based co-ligands explored as candidates for complementary cluster formation with TBC[4].

General cluster core structure for 1-4: Reaction of TBC[4], a $SaoH_2$-based co-ligand candidate (**IV – VII**) and either $MnCl_2$ or $Mn(NO_3)_2$ hydrates in a basic dmf / MeOH solvent mixture (this high polarity medium is used to ensure a homogenous solution is obtained) resulted in formation of four $Mn^{III}_7Mn^{II}$ clusters. As all four complexes have the same general structure, and in the interest of brevity, we describe the structural characteristics common to **1**–**4** using **1** (Fig. 3) as a representative example prior to highlighting notable differences between each complex. Structural analysis of single crystals of **1-4** reveals that the metallic skeleton is a novel $[Mn_8]$ cluster where a buckled $[Mn^{III}_5Mn^{II}]$ triangle of triangles has been capped top and bottom by $[Mn^{III}TBC[4]]^-$ moieties. Three di-anionic Sao^{2-} ligands and other coordinating ligands

(e.g. bridging methoxide) support the central belt of six manganese ions.

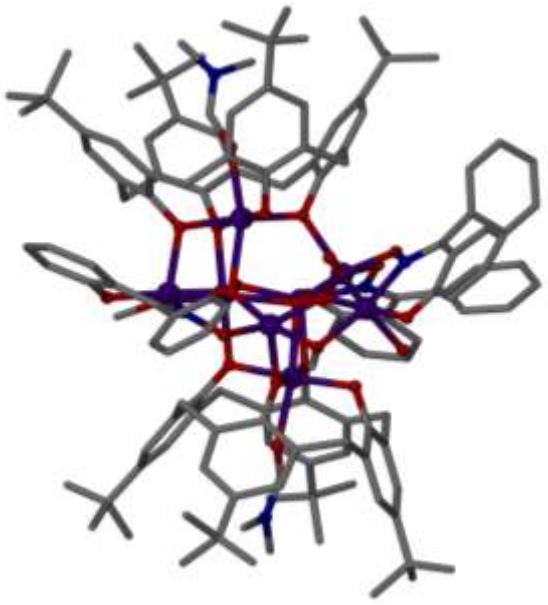

Figure 3. Single crystal X-ray structure of **1** showing the buckled $Mn^{III}_5Mn^{II}$ plane, capped on top and bottom by $[Mn^{III}TBC[4]]^-$ moieties. Non-coordinating solvents and H atoms are omitted for clarity. Color code: C grey; O red; N blue; Mn purple.

$[Mn^{III}_7Mn^{II}(TBC[4]\text{-}4H)_2(IV^{-2})_3(\mu_4\text{-}O^{2-})_2(\mu_3\text{-}O^{2-})(dmf)_2(\mu_2\text{-}MeO^-)_2(\mu_2\text{-}OH^-)(H_2O)_2]\cdot 6dmf\cdot H_2O$, 1: Inspection of the structure of **1** reveals that each type of ligand retains its expected bonding mode within the new cluster formed. Each tetra-anionic TBC[4] houses a Mn^{III} ion in the center of the polyphenolic cavity, and each doubly deprotonated **IV** ($PhSao^{2-}$) bridges two Mn^{III} ions via Mn-N-O-Mn coordination. The metallic skeleton (Fig. 4A) is shown alongside a top-down view of the distorted $[Mn^{III}_5Mn^{II}]$ plane for clarity (Fig. 4B); the Mn1 – Mn4 and Mn6 – Mn8 ions are all in the +3 oxidation state, while Mn5 is the only Mn^{II} ion in the assembly. Mn7 is bound centrally to the four oxygen atoms of one fully deprotonated TBC[4] and this occurs with Mn7-O1, Mn7-O2, Mn7-O3 and Mn7-O4 distances in the range of 1.925(7) – 1.984(7) Å. The coordination sphere of Mn7 is completed by a μ_4-oxide (Mn7-O18, 2.300(8) Å) and a ligated dmf (Mn7-O15, 2.241(8) Å), both of which define the Jahn-Teller axis. O3 is terminally bound to Mn7, whereas O1, O2 and O4 bridge to Mn5, Mn2 and Mn4 respectively (Mn5-O1, 2.174(8) Å, Mn2–O2, 2.203(8) Å and Mn4–O4, 2.099(7) Å). Mn5 is also bonded to O5 from the second tetra-anionic TBC[4] with a Mn5-O5 distance of 2.186(8) Å. As is the case for Mn7, Mn3 is located in the center of the second tetra-anionic TBC[4] binding cavity (Mn3-O5, Mn3-O6, Mn3-O7 and Mn3-O8 distances in the range of 1.920(7) – 1.968(7) Å) and has a Jahn-Teller axis defined by a μ_4-oxide (Mn3-O17, 2.329(7) Å) and a ligated dmf (Mn3-O16, 2.201(9) Å).

As mentioned above, the rather complex bonding / topology found in the distorted $[Mn^{III}_5Mn^{II}]$ belt of atoms (Fig. 4B) is general for **1** – **4**. Within this belt, Mn8 has distorted octahedral geometry, with two water ligands (Mn8-O23, 2.201(7) Å and Mn8-O24, 2.330(8) Å) defining the Jahn-Teller axis. A μ–methoxide links Mn8 and Mn1 with Mn8-O21 and Mn1-O21 distances of 1.971(8) Å and 1.943(8) Å respectively. In addition, a μ_3-oxide links Mn8, Mn1 and Mn2 with Mn-O19 distances in the range of 1.859(8) – 1.903(8) Å. The coordination sphere of Mn8 is completed by terminal bonding to the phenolic oxygen and oximic nitrogen atoms of a dianionic **IV** (O11/N2/O12 in Fig. 4B), with Mn8-O11 and Mn8-N2 distances of 1.856(8) Å and 1.985(10) Å respectively. This dianionic **IV** connects to square pyramidal Mn2 via its oximic oxygen atom with a Mn2-O12 distance of 1.928(8) Å. The coordination sphere of Mn2 is completed by an oximic oxygen atom of a second dianionic **IV** (O10/N1/O9 in Fig. 4B) and a μ_4-oxide (Mn2-O10, 1.926(8) Å and Mn2-O17, 1.898(7) Å respectively). The same μ_4-oxide (O17) bridges to both Mn6 and Mn5 with respective Mn6-O17 and Mn5-O17 distances of 1.903(7) and 2.203(7) Å. Mn6 bonds to the phenolic oxygen and oximic nitrogen of the dianionic O10/N1/O9 **IV** (Mn6-O9, 1.873(7) Å and Mn6-N1, 1.96(10) Å) and the coordination sphere is completed by μ-hydroxide that links to Mn5 (Mn6-O22, 1.942(7) Å and Mn5-O22, 2.107(8) Å).

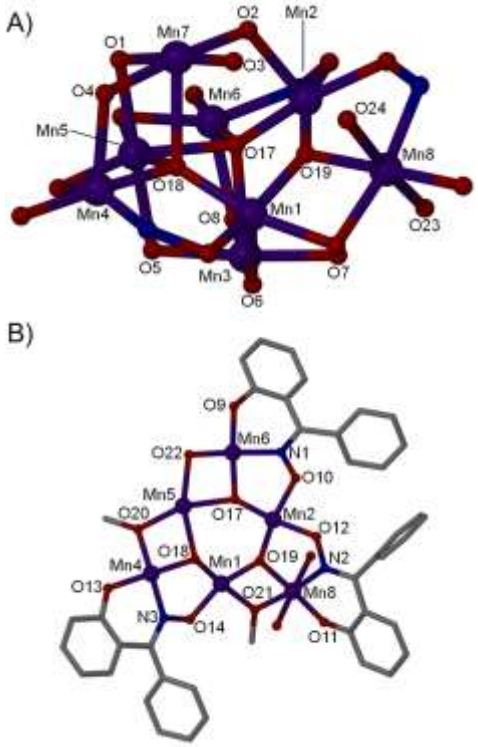

Figure 4. A) Polymetallic skeleton highlighting the coordination environments of Mn ions in **1**. B) Distorted $[Mn^{III}_5Mn^{II}]$ plane found in **1**. Atoms selectively labelled to aid discussion. Color code: C grey; O red; N blue; Mn purple. H atoms and other parts of the structure omitted for clarity.

Mn5 has distorted octahedral geometry and is connected to square pyramidal Mn4 via a μ–methoxide (Mn5-O20, 2.075(7) Å and Mn4-O20, 1.897(7) Å) and a μ_4-oxide (Mn5-O18, 2.211(7) Å and Mn4-O18, 1.897(7) Å). In addition to the Mn4-O4 coordination described above for the first TBC[4] tetra-anion, the coordination sphere of Mn4 is completed by bonding to phenolic oxygen and oximic nitrogen atoms of the third dianionic **IV** (O13/N3/O14 in Fig. 4B), with Mn4-O13 and Mn4-N3 distances of 1.863(7) and 1.968(9) Å respectively. Finally, the O13/N3/O14 oximic oxygen (O14) and the O18 μ_4-oxide both coordinate to square pyramidal Mn1 (Mn1-O14 and Mn1-O18 distances of 1.928(8) and 1.874(7) Å respectively). With respect to the generic nature of the cluster core topology found in **1** – **4** (**1** $PhSao^{2-}$; **2** 3-iPr-Sao^{2-}; **3** 3-Et-Sao^{2-}; **4** 3-Me-Sao^{2-}) it should be noted that some small differ-

ences are observed in the identity of peripheral ligands around the distorted six ion [$Mn^{III}_5Mn^{II}$] plane. In the bridging positions, these are all either μ-methoxide or μ-hydroxide, and are all either methanol or water in the analogous position to the Jahn-Teller axis of Mn3 in **1**. In addition, in **4** one Mn ion and the attached dianionic **VII** are each disordered over two positions, and this was modelled with crystallographic occupancies of 0.75 and 0.25 respectively.

General cluster core structure 5-8: Reaction of TBC[4], **II** or **III** and either $MnCl_2$ or $Mn(NO_3)_2$ hydrates (figure 5A shows **5** as a representative structure of **5-8**) in a basic solvent system of dmf / MeOH also resulted in formation of four new [$Mn^{III}_7Mn^{II}$] clusters (**II** ($MeSaoH_2$) affords **5** and **6**, whilst **III** ($EtSaoH_2$) affords **7** and **8**). All four complexes conform to the same basic core structure as **1-4**, highlighting the structural persistence of the Mn_8 cluster. Two key differences between **5-8** and **1-4** are found in the location of the unique Mn^{II} ion (Mn7 in **5**, Fig. 5B, and the equivalent position in **6-8**) and in the incorporation of a chloride or nitrate (dependent on reaction conditions) into the central six ion plane.

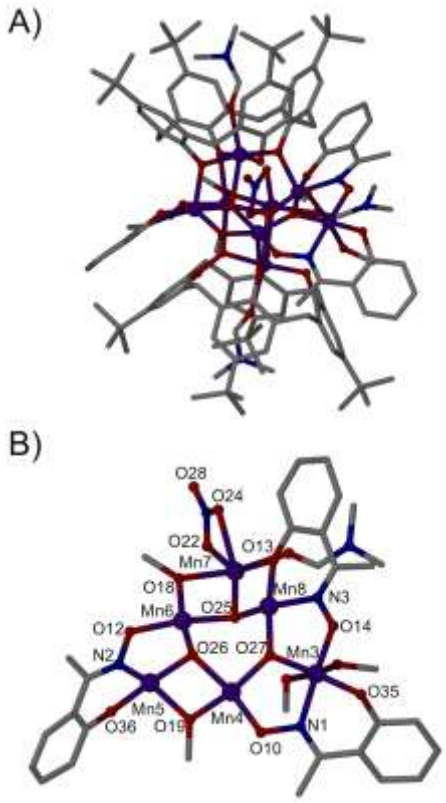

Figure 5. A) Single crystal X-ray structure of **5**. B) Coordination environment around distorted [$Mn^{III}_5Mn^{II}$] plane. Non-coordinating solvents and H atoms omitted for clarity. Color code: C grey; O red; N blue; Mn purple.

The [$Mn^{III}_5Mn^{II}$] moieties in **5-8** are slightly different, as is the case in **1-4**, and these small differences are generally manifested in the peripheral ligands around the manganese ions (combinations of terminal water, methanol and dmf). In **5** and **6** Mn5 is bonded to a dmf ligand, which is presumably a consequence of the specific oxime used for cluster formation (**II** along with **VII** are the $SaoH_2$ ligands with the smallest substituents to result in a Mn_8 complex in this study, although **VII** results in the alternative Mn_8 cluster topology). The main difference is that a nitrate ion is coordinated to Mn7 in **5**. The equivalent position in **7** is also occupied by nitrate and in **6** and **8** it is occupied by a chloride ligand.

Mn_8 clusters are relatively common in the literature,[10] and a search of the Cambridge Structural Database reveals *ca*. 90 entries which encompass a variety of topologies and oxidation state distributions. However to our best knowledge **1-8** represent the first examples of [$Mn^{III}_7Mn^{II}$] clusters and exhibit a unique metallic skeleton. Both factors are linked to the preferred metal-ion binding properties of the ligands employed (TBC[4] preferentially binds Mn^{III} and Sao^{2-} ligands generally adopt architectures based upon Mn^{III}_3 triangles).[5]

Structural comparison of the [$Mn^{III}_5Mn^{II}$] skeleton

Schematics of the generic [$Mn^{III}_5Mn^{II}$] moieties obtained in **1-4** and **5-8** are given in Figure 6. Simple inspection reveals that one key difference is the position of the unique Mn^{II} ion. In **1-4** the Mn^{II} lies in a position at the midpoint along an edge of the horizontal [$Mn^{III}_5Mn^{II}$] plane, whereas in **5-8** it occupies a corner position. This naturally results in different magnetic exchange interactions within each custer type. The relative position of the Sao^{2-} ligands observed in the two cluster skeletons is also different. In Figure 6A each of the corner manganese ions is coordinated to the phenolic oxygen of a Sao^{2-} ligand. In Figure 6B this is not the case, and position 3 is involved in coordination to either a chloride or nitrate ion. The reason for this is unknown, however the nature of the oxime subtituent appears to be important.

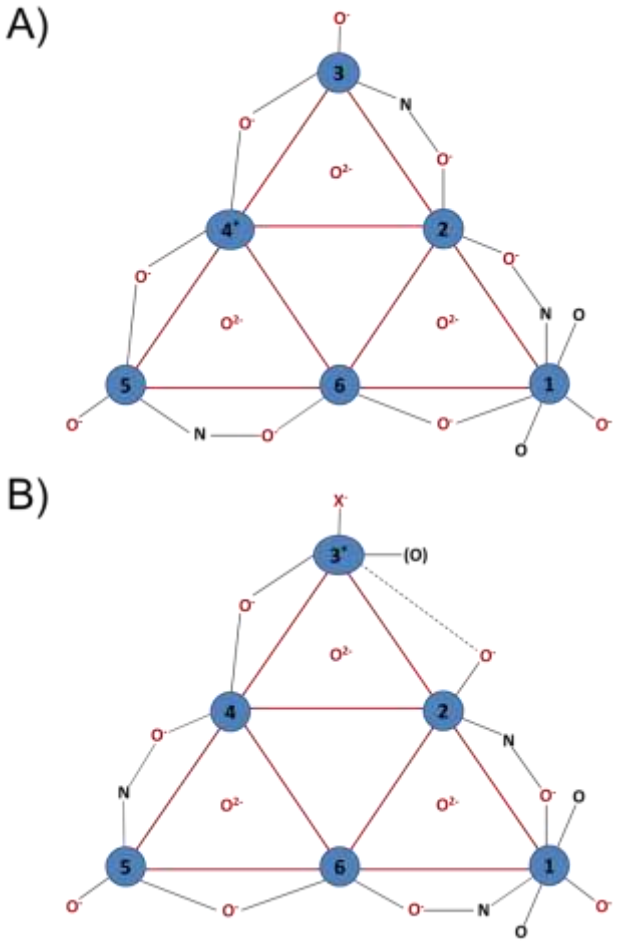

Figure 6. Generic schematic and Mn ions in the buckled [$Mn^{III}_5Mn^{II}$] planes observed in **1-4** (A) and **5-8** (B). Mn^{II} positioning is indicated by *. X = Cl^- or NO_3^-.

In **1** the substituent is a relatively large phenyl group attached to the oximic carbon atom. The substituents in **2**-**4** are methyl, ethyl or isopropyl groups attached to the aromatic skeleton, and therefore the spacial arrangement of each substituent is relatively well defined due to the rigidity of the phenyl ring. The substituents in **5**-**8** are methyl or ethyl groups attached to the oximic carbon atom, and are therefore in a comparitively flexible environment, potentially allowing subsequent coordination of a chloride or nitrate ion. This effect is perhaps precluded in **1** due to the relative size of a phenyl substituents w.r.t methyl or ethyl groups.

From inspection of the collated structural data from analysis of **1**-**8** it is clear that the [$Mn^{III}_5Mn^{II}$] belt is non-planar in each case. Given this, several structural parameters were measured to quantify this non-planarity and thus the degree of similarity between each complex (full details in Supporting Information, Table S1). In general, the distances between Mn ions remain relatively consistent across the series of compounds, and the corners of the [$Mn^{III}_5Mn^{II}$] moiety correspond very closely to an equilateral triangle. It is evident that the "buckling" of the plane of Mn ions is mainly manifested in the positions where the α parameter varies significantly from 0°, although the C[4] ligands have been tethered of the metals midway between the corners of each edge of the triangle. A parameter Δ_n has been used to describe the lateral displacement of each Mn_n ion from a least-squares plane through Mn1-Mn3-Mn5.[11] In all cases Δ_2 has the largest value (range of 0.900 Å – 1.002 Å). Δ_4 has a relatively small displacement of less than 0.2 Å in each case, a consequence of coordination to both TBC[4] tetra-anions, and Δ_6 is displaced from the least-squares plane by between 0.565 Å and 0.916 Å. The fact that Δ_2 and Δ_6 are out-of-plane explains another structural effect in **1**-**8** causing the TBC[4] tetra-anions to point in opposite directions. Least-squares planes containing the oxygen atoms of each TBC[4] can be calculated, and the dihedral angle (α) between these measured. The α parameter varies from 15.14˚ – 22.62˚ and is therefore reasonably consistent across the series of complexes. Analysis of TBC[4] complexes containing manganese reveals that α is normally close to 0˚,[7b,c] emphasizing the considerable effect of the co-ligand on cluster formation here. The exchange of a Ln^{III} for a Mn^{II} ion in [$Mn^{III}_2Mn^{II}_2$(TBC[4])$_2$] leads to a less symmetric cluster with an α value of 7°, still smaller than in **1**-**8**.[7i] Other examples exist at the methylene bridge, somewhat constraining the bonding geometry.[10a,12] It was previously reported that magnetic exchange interactions within Sao^{2-}-based clusters can be modulated through variation of the Mn-N-O-Mn torsion angle.[5] These torsion angles (τ) were measured for every Sao^{2-} in each of the complexes **1**-**8.** While it is difficult to draw definitive conclusions for such complex multicomponent systems, it is clear that τ_{mean} in **1**-**4** (10.81˚ – 22.16˚) is considerably smaller than that in **5**-**8** (23.20˚ – 31.42˚). This fact can perhaps be explained by consideration that **5**-**8** incorporate an additional bulky chloride or nitrate anion in the resulting assembly.

[$Mn^{IV}_2Mn^{III}_2(X^{2-})_6(X(imine)^{2-})_2$]·dmf·6MeOH,9: In contrast to successful formation of Mn_8 clusters with oxime ligands **II**–**VII**, analogous reactions with **X** afforded the new [$Mn^{IV}_2Mn^{III}_2$] cluster shown in Figure 7. The asymmetric unit contains half of the title formula of **9**, which upon symmetry expansion reveals a [$Mn^{IV}_2Mn^{III}_2$] cluster supported by six dianionic **X** ligands and two related imine ligands. The magnetic core of **9** is best described as a zig-zag chain of four Mn ions. Mn1 and its symmetry equivalent (s.e., Mn1') have octahedral geometry and are in the 4+ oxidation state. Three fully deprotonated **X** ligands occupy the coordination sphere of Mn1: both the phenolic oxygen atoms (O1, O3 and O5, Mn1-O distances in the range of 1.865(3) – 1.868(3) Å) and the oximic nitrogen atoms (N1, N2 and N3, Mn1-N distances in the range of 1.982(3) – 1.996(3) Å) coordinate in a *fac* fashion (Fig. 7A). The oximic oxygen atoms of the dianionic **X** ligands further bridge to the distorted octahedral Mn^{III} ions, Mn2 and Mn2'. O2 and O4 are terminally bound to Mn2 (Mn2-O2, 1.938(3) Å and Mn2-O4, 2.121(3) Å), whilst O6 bridges Mn2 and Mn2' (Mn2-O6, 1.948(3) Å and Mn2'-O6, 2.357(3) Å). Mn2 and its s.e. are in the 3+ oxidation state, with Jahn-Teller axes defined by the O4-Mn2-O6' or corresponding O4'-Mn2'-O6 vectors. The two remaining coordination sites of Mn2 are occupied by the phenolic oxygen and nitrogen of the imine moiety (Mn2-O7, 1.869(3) Å and Mn2-N4, 1.974(3) Å). While there is nothing remarkable about the bond lengths found in **9** there are two main points of interest. First, the presence of two Mn^{IV} ions (resulting from a two electron oxidation from the Mn^{II} starting material) is important from a magnetic perspective, *vide infra*. Although the presence of Mn^{IV} is not a rare occurrence in polynuclear manganese chemistry, its comparatively large and antiferromagnetic exchange interactions with Mn^{III} typically result in higher lying exited states than Mn^{III}–Mn^{III} or Mn^{III}–Mn^{II} exchange interactions, which is a desirable property for SMM behaviour.[13] Secondly, from a synthetic point of view, the reduction of two oxime ligands to the corresponding imine during cluster formation is interesting and relatively rare for salicylaldoximes.[14] The nature of this transformation is not known and may be related to the varied redox chemistry of manganese, proceeding via an initial metal mediated oxygen transfer of the oxime ligand. Interestingly **X** has been used before to construct either $Mn^{IV}_2Mn^{III}$ clusters or Mn^{III}_3 single-chain magnets,[15] albeit in these cases the oximate ligands are retained and are not reduced to the corresponding imine.

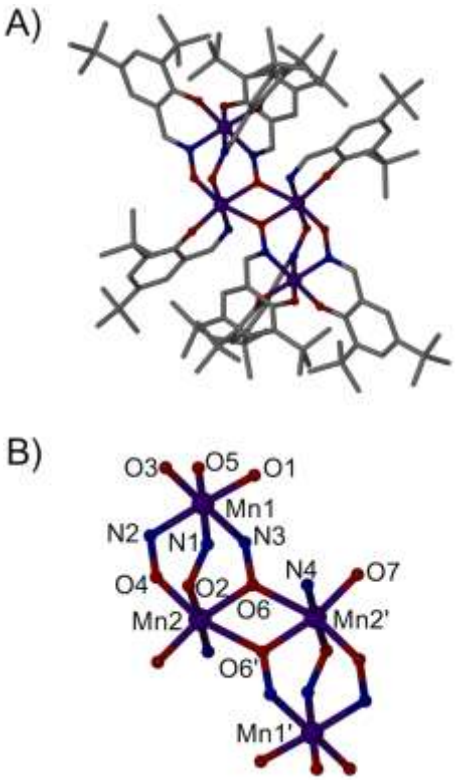

Figure 7. A) Single crystal X-ray structure of **9**. Non-coordinating solvents and H atoms omitted for clarity. B) Polymetallic skeleton and coordination spheres of Mn atoms in **9**. Atoms selectively labelled to aid discussion. Color code: C grey; O red; N blue; Mn purple.

Steric effects of co-ligands on cluster formation: In compound **9**, the fact that a Mn_4 was isolated as the only product rather than a Mn_8 cluster prompted further consideration. The co-ligand X possesses a tertiary butyl group adjacent to the phenolic oxygen atom, and it is postulated that the steric demands of this group are too large to permit Mn_8 cluster formation with TBC[4] as an additional bulky co-ligand. Partial space-filling diagrams of **1**, **2** and **3** (Figure 8) indicate that this may well be the case. In **1** the phenyl rings of the oxime and the TBC[4] tetra-anion are approximately co-planar and the phenyl substituent points away from the cluster core, suggesting that there is no steric impediment to assembly. Similarly, in **3** the ethyl substituent adjacent to the phenolic oxygen is sufficiently small that it does not appear to interfere with cluster formation; it is positioned so as to form a complementary CH… π interaction as shown in Fig. 8B. In **2** the methyl groups of the isopropyl group point away from the cluster, again leaving a hydrogen atom pointing towards an aromatic ring of the calixarene (Fig. 8C). Extending this argument to include a methyl group in place of the hydrogen atom of an isopropyl group, i.e. being ^{t}Bu as in **IX** or **X**, would necessitate a methyl group pointing directly towards the calixarene. The structure of **2** (Fig. 8C) suggests that there is insufficient space for this to occur, and so any cluster formation would likely proceed via an alternative pathway, that is, giving a C[4]-supported $Mn^{III}_2Mn^{II}_2$ cluster with **IX** and an oxime/imine-supported $Mn^{IV}_2Mn^{III}_2$ cluster with **X**.

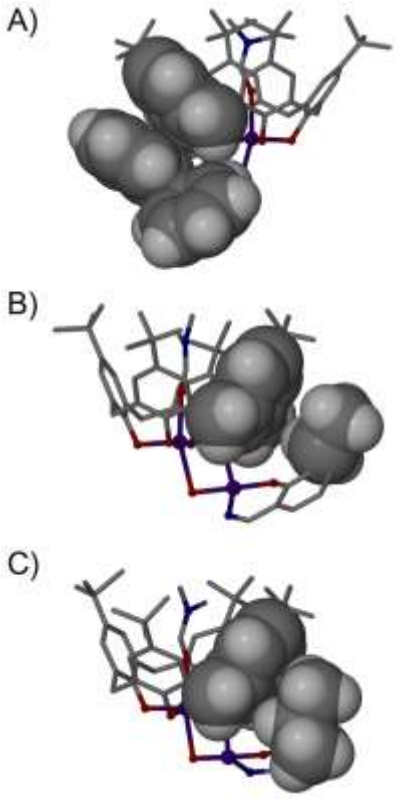

Figure 8. Sections of the single crystal X-ray structures of **1** (A), **3** (B) and **2** (C) shown in partial space-filling representations to illustrate the steric requirements of co-ligand substituents. Color code: C grey; O red; N blue; Mn purple. H atoms and other parts of the structure omitted for clarity.

Magnetic properties: The dc (direct current) molar magnetic susceptibility, χ_M, of polycrystalline samples of **1**, **3**, **4**, **5**, **6** and **9** (representative examples of the different structure types) were measured in an applied magnetic field, *B*, of 0.1 T, over the T = 2-300 K temperature range. The experimental results are shown in Figures 9-10 in the form of the $\chi_M T$ product versus T, where $\chi_M = M / B$, and M is the magnetization of the sample.

The octametallic species can be divided into two distinct families whose structures differ in the position of the Mn(II) ion, complexes **1**-**4** (type A) and **5**-**8** (type B), as depicted in Figure 6. At room temperature, the $\chi_M T$ product of all five compounds is approximately 25 cm^3 K mol^{-1} (Figure 9), in good agreement with the sum of Curie constants for a $[Mn^{III}_7Mn^{II}]$ unit (25.875 cm^3 K mol^{-1}, g = 2.0). Upon cooling, the $\chi_M T$ products remain relatively constant until T ~ 200 K where the data diverges: decreasing slowly to values close to 10 cm^3 K mol^{-1} for **1**, **3** and **4** at 2 K, but increasing for **5** and **6** to maximum values of 37 and 33 cm^3 K mol^{-1}, respectively, at T = 15 K. This behavior is consistent with competing (weak) ferro- and antiferromagnetic exchange interactions in both cases, but where the metal topology in structure type B gives rise to the stabilization of a larger 'spin ground state' than that for structure type A. The decrease in $\chi_M T$ below 15 K for **5** and **6** can be attributed to zero-field splitting effects and/or the presence of antiferromagnetic inter-molecular interactions. The large nuclearity and complex topology of these $[Mn^{III}_7Mn^{II}]$ species prevents any quantitative analysis of exchange constants, and we note that $|J|$ is likely of the same magnitude as $|D_{Mn(III)}|$ resulting in a band of closely spaced spin states in each case, rendering the notion of an isolated "*S*" ground state moot. This is in-line with previous measurements of calix[*n*]arene and oxime-based Mn clusters with Mn(III/II) ions bridged by hydroxide, alkoxide and -N-O- atoms, where $|J| \leq 5$ cm^{-1}.[5d,7i] Low temperature variable-temperature-and-variable-field (VTVB) magnetization data collected in fields of up to B = 7 T (Figure S1) are also consistent with this picture, with M increasing in a near linear fashion with B for all five complexes. Both **5** and **6** display frequency-dependent signals in out-of-phase (χ_M'') ac susceptibility (Figure S2), suggestive of slow relaxation of the magnetization and SMM behavior. Data obtained by varying the frequency of oscillation of the ac field were fit to the Arrhenius equation, affording U_{eff} = 26.1, 28.5 K and τ = 9.63 x 10^{-9}, 1.45 x 10^{-9} s for **5**, **6**, respectively.

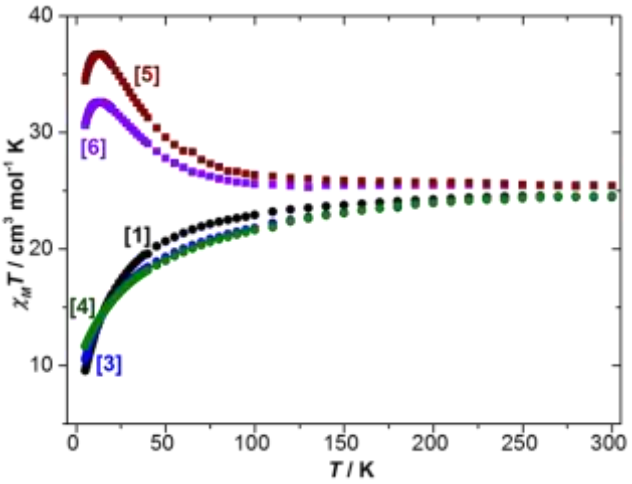

Figure 9. Plot of $\chi_M T$ versus T for complexes **1** and **3**-**6** measured in the T = 300 – 2 K temperature range in an applied magnetic field of B = 0.1 T.

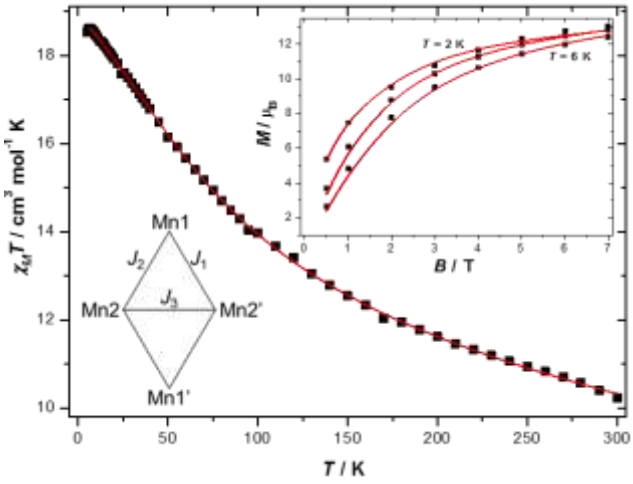

Figure 10. Plot of $\chi_M T$ versus T for complex **9** measured in the T = 300 – 2 K temperature range in an applied magnetic field of B = 0.1 T. The solid line is a fit of the experimental data to the isotropic part of spin-Hamiltonian (1) using the exchange coupling scheme in the inset (bottom left). The top right inset shows the magnetization data for T = 2, 4, 6 K. The red lines are a fit of the experimental data to spin-Hamiltonian (1) with the J values fixed to the values extracted from the susceptibility.

At room temperature, the $\chi_M T$ product of the tetrametallic species **9** has a value of ~10 cm^3 K mol^{-1} (Figure 10), in good agreement with the sum of Curie constants for a [$Mn^{IV}_2Mn^{III}_2$] unit (9.75 cm^3 K mol^{-1}, g = 2.0). Upon cooling, the $\chi_M T$ product of **9** increases, reaching a maximum value of ~19 cm^3 K mol^{-1} at T = 2 K. This behavior is suggestive of the presence of both ferro- and antiferromagnetic exchange interactions being present. Inspection of Figure 7 reveals that there are three distinct interactions present in complex **9**, whose structure is that of a distorted butterfly, with the Mn(IV) ions on the wing-tips and the Mn(III) ions in the body positions. Mn1 is connected to Mn2' (J_1) through three Mn-N-O-Mn oxime bridges and to Mn2 (J_2) by just one Mn-N-O-Mn oxime bridge. Mn2 is connected to Mn2' (J_3) by two O-atom(oxime) bridges. Isotropic fitting the experimental susceptibility data to the model in the inset of Figure 10 and spin-Hamiltonian (1) affords the best fit parameters J_1 = +6.62 cm^{-1}, J_2 = +12.92 cm^{-1}, J_3 = -8.36 cm^{-1}, with g fixed at g = 2.0.

$$\hat{H} = \mu_B B \sum_i g_i \hat{S}_i - 2 \sum_{i,j<i} J_{ij} \hat{S}_i \cdot \hat{S}_j + \sum_i D_i \left[\hat{S}^2_{i,z} - S_i(S_i+1)/3 \right] \qquad (1)$$

A fit of the magnetization data (Figure 10, inset) with these J values fixed, and maintaining g = 2.0, gives $D_{Mn(III)}$ = -4.4 cm^{-1}. J_1 and J_2 are consistent with the exchange reported in a mixed-valent c[8]/oxime-based Mn(III/IV) dimer where J = +9.81 cm^{-1}.[8] Magneto-structural correlations recently developed for alkoxide-bridged [$Mn^{III}_2O_2$] dimers revealed the importance of the orientation of the JT axis in determining both the sign and magnitude of the exchange interaction.[16] Indeed in all cases where the JT axes were aligned parallel to each other but perpendicular to the bridging [$Mn^{III}_2O_2$] plane, as here, the interaction was found to be weakly antiferromagnetic with J values ranging from −8.2 cm^{-1} to −15.5 cm^{-1}, consistent with J_3. Ac susceptibility measurements on **9** reveal the presence of frequency-dependent χ_M'' signals (Figure 11) indicative of slow relaxation of the magnetization and SMM behavior, with U_{eff} = 28.4 K and τ = 6.85 x 10^{-9} s.

CONCLUSIONS

This work demonstrates the synthesis of eight new $Mn^{III}_7Mn^{II}$ clusters and one new $Mn^{IV}_2Mn^{III}_2$ cluster, by the complementary combination of C[4] and $SaoH_2$ ligands. The characteristic bonding modes of each ligand type is present in the resultant complexes. Furthermore, variation of the steric properties of the $SaoH_2$ ligand leads to different metallic core topologies and oxidation state distributions. The magnetic properties of the $Mn^{III}_7Mn^{II}$ clusters can thus be fine-tuned by simple ligand modification, with one structure type (B) displaying SMM behavior and the other (A) not. In the case of the $Mn^{IV}_2Mn^{III}_2$ cluster the large steric requirement imposed by two bulky tBu groups leads to a radically different complex that exhibits competing ferro- and antiferromagnetic exchange interactions and slow relaxation of the magnetization. The protocol of ligand complementarity is therefore demonstrated as an important strategy in the design of large polymetallic architectures and importantly, in the quest for complexes possessing enhanced or targeted magnetic properties.

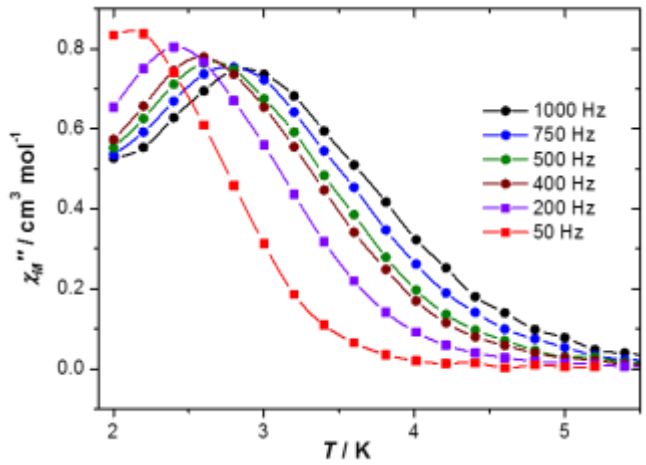

Figure 11. Plot of the out-of-phase ac susceptibility (χ_M'') versus temperature for complex **9** at the indicated frequencies.

Experimental

TBC[4][6] and ligands **I** – **X**[5] were synthesized according to literature procedures. Crystallographic data were collected on a Bruker Apex II Diffractometer operating with Mo-Kα radiation (0.71073 Å) at 100(2)K.

$[Mn^{III}_7Mn^{II}(TBC[4]\text{-}4H)_2(IV^{2-})_3(\mu_4\text{-}O^{2-})_2(\mu_3\text{-}O^{2-})(dmf)_2(\mu_2\text{-}MeO^-)_2(\mu_2\text{-}OH^-)(H_2O)_2]\cdot 6dmf\cdot H_2O$, 1: TBC[4] (100 mg, 0.154 mmol), 2-hydroxybenzophenone oxime (66 mg, 0.308 mmol) and $Mn(NO_3)_2\cdot 4H_2O$ (232 mg, 0.924 mmol) were dissolved in dmf / MeOH (8mL / 8mL) and stirred for ten minutes. Triethylamine (1.54 mmol, 0.21 mL) was added and the resulting dark brown solution was stirred for a further hour before the mixture was filtered. Dark brown crystals of **1** were grown by slow evaporation of the mother liquor over several days. Yield (based on TBC[4]): 91 mg, 38%. $C_{153}H_{200}N_{11}Mn_8O_{31}$: calcd. C 58.73; H 6.44; N 4.92; found C 57.90; H 6.19; N 4.68%. **Crystal data (CCDC 1555660):** $C_{153}H_{200}Mn_8N_{11}O_{31}$, M =3128.76 g/mol, monoclinic, space group $P2_1/n$ (no. 14), a = 22.19(6) Å, b = 21.12(5) Å, c = 31.66(8) Å, β = 91.96(8)°, V = 14824(61) Å^3, Z = 4, 85392 reflections measured, 14005 unique (R_{int} = 0.1446) which were used in all calculations. The final R_1 was 0.0615 (>2sigma(I)) and wR_2 was 0.1589 (all data).

$[Mn^{III}_7Mn^{II}(TBC[4]\text{-}4H)_2(V^{2-})_3(\mu_4\text{-}O^{2-})_2(\mu_3\text{-}O^{2-})(dmf)_2(\mu_2\text{-}MeO^-)_3(H_2O)(MeOH)]$, 2: TBC[4] (100 mg, 0.154 mmol), 3-isopropyl-salicylaldoxime (55 mg, 0.308 mmol) and $Mn(Cl)_2\cdot 4H_2O$ (183 mg, 0.924 mmol) were dissolved in a solvent mixture of dmf / MeOH (8mL / 8mL) and stirred for 10 minutes. Triethylamine (1.54 mmol, 0.21 mL) was added and the mixture changed Color from pale pink to dark brown. After stirring for a further hour, the reaction was filtered and dark brown crystals of **2**, suitable for single-crystal X-ray diffraction studies, were grown by slow evaporation of the mother liquor. Crystalline samples were contaminated with **V**, precluding calculation of an accurate yield and the study of the magnetic properties. Although this is the case, the structure of **2** has been included here to aid discussion of the steric factors in determining cluster type. **Crystal data (CCDC 1555661):** $C_{128}H_{166}Mn_8N_5O_{24}$, M =2598.17 g/mol, monoclinic, space group $P2_1/c$ (no. 14), a = 24.654(3) Å, b = 21.946(2) Å, c = 30.893(3) Å, β = 103.802(3)°, V = 16232(3) Å^3, Z = 4, 16906 reflections measured, 16906 unique (R_{int} = 0.0000, merged) which were used in all calculations. The final R_1 was 0.0801 (I > 2σ(I)) and wR_2 was 0.2466 (all data).

$[Mn^{III}_7Mn^{II}(TBC[4]\text{-}4H)_2(VI^{2-})_3(\mu_4\text{-}O^{2-})_2(\mu_3\text{-}O^{2-})(dmf)_2(\mu_2\text{-}MeO^-)_3(MeOH)_{1.5}(H_2O)_{0.5}]\cdot 2dmf$, 3: TBC[4] (100 mg, 0.154 mmol), 3-ethyl-salicylaldoxime (51 mg, 0.308 mmol) and $Mn(NO_3)_2\cdot 4H_2O$ (232 mg, 0.924 mmol) were dissolved in a mixture of dmf / MeOH (8mL / 8mL). After stirring for 10 minutes, triethylamine (1.54 mmol, 0.21 mL) was added and the resulting dark brown solution was stirred for a further hour. The reaction was filtered and dark brown crystals of **3** were grown by slow evaporation of the mother liquor over several days. Yield (based on TBC[4]): 58 mg, 27%. $C_{131.5}H_{175}N_7Mn_8O_{26}$: calcd. C 58.30; H 6.51; N 3.62; found C 57.68; H 6.39; N 3.68%. This difference is attributed to solvent loss and disorder within the crystal, precluding accurate calculation of the former. **Crystal data (CCDC 1555662):** $C_{131.5}H_{175}Mn_8N_7O_{26}$, M =2709.31 g/mol, monoclinic, space group $P2_1/n$ (no. 14), a = 20.45(9) Å, b = 32.73(13) Å, c = 22.39(9) Å, β = 112.39(6)°, V = 13857(98) Å^3, Z = 4, 68260 reflections measured, 18453 unique (R_{int} = 0.1455) which were used in all calculations. The final R_1 was 0.0911 (>2sigma(I)) and wR_2 was 0.2744 (all data).

$[Mn^{III}_7Mn^{II}(TBC[4]\text{-}4H)_2(VII^{2-})_3(\mu_4\text{-}O^{2-})_2(\mu_3\text{-}O^{2-})(dmf)_2(\mu_2\text{-}MeO^-)_3(MeOH)(H_2O)]\cdot 0.25H_2O$, 4: TBC[4] (100 mg, 0.154 mmol), 3-methyl-salicylaldoxime (47 mg, 0.308 mmol) and $Mn(NO_3)_2\cdot 4H_2O$ (232 mg, 0.924 mmol) were dissolved in dmf / MeOH (8mL / 8mL) and stirred for 10 minutes. Triethylamine (1.54 mmol, 0.21 mL) was added and the dark brown solution was stirred for a further hour. The reaction was filtered and dark brown crystals of **4**, suitable for single-crystal X-ray diffraction studies, were grown by slow evaporation of the mother liquor. Yield (based on TBC[4]): 67 mg, 24%. $C_{122}H_{151}N_5Mn_8O_{24}$: calcd. C 58.36; H 6.06; N 2.79; found C 59.05; H 6.45; N 3.49%.%. This difference is attributed to solvent loss and disorder within the crystal, precluding accurate calculation of the former. **Crystal data (CCDC 1555663):** $C_{122}H_{154.5}Mn_8N_5O_{24.25}$, M =2518.52 g/mol, monoclinic, space group $P2_1/n$ (no. 14), a = 19.5613(16) Å, b = 31.705(3) Å, c = 23.5099(16) Å, β = 112.680(3)°, V = 13453.1(18) Å^3, Z = 4, 18427 reflections measured, 18427 unique (R_{int} = 0.0750) which were used in all calculations. The final R_1 was 0.0873 (I > 2σ(I)) and wR_2 was 0.2703 (all data).

$[Mn^{III}_7Mn^{II}(TBC[4]\text{-}4H)_2(II^{2-})_3(\mu_4\text{-}O^{2-})_2(\mu_3\text{-}O^{2-})(dmf)_3(\mu_2\text{-}MeO^-)_2(NO_3^-)(MeOH)_{1.5}(H_2O)_{0.5}]$, 5: TBC[4] (100 mg, 0.154 mmol), 2-hydroxyacetophenone oxime (46 mg, 0.308 mmol) and $Mn(NO_3)_2\cdot 4H_2O$ (232 mg, 0.924 mmol) were dissolved in dmf / MeOH (8mL / 8mL) and the mixture was stirred for 10 minutes. Triethylamine (1.54 mmol, 0.21 mL) was added and the dark brown solution was stirred for an additional hour. The reaction mixture was filtered and dark brown crystals of **5**, suitable for single-crystal X-ray diffraction studies, were grown by slow evaporation of the mother liquor. Yield (based on TBC[4]): 42 mg, 21%. $C_{124.5}H_{156.5}N_7Mn_8O_{27}$: calcd. C 57.02; H 6.01; N 3.74; found C 55.67; H 6.45; N 5.54%. This difference is attributed to solvent loss and disorder within the crystal, precluding accurate calculation of the former. **Crystal data (CCDC 1555664):** $C_{124.5}H_{159}Mn_8N_7O_{27}$, M =2625.10 g/mol, monoclinic, space group $P2_1/n$ (no. 14), a = 21.16(4) Å, b = 21.80(4) Å, c = 33.97(6) Å, β = 93.63(5)°, V = 15635(54) Å^3, Z = 4, 28606 reflections measured, 28606 unique (R_{int} = 0.0000, merged) which were used in all calculations. The final R_1 was 0.1130 (I > 2σ(I)) and wR_2 was 0.3270 (all data)

$[Mn^{III}_7Mn^{II}(TBC[4]\text{-}4H)_2(II^{2-})_3(\mu_4\text{-}O^{2-})_2(\mu_3\text{-}O^{2-})(dmf)_{3.5}(\mu_2\text{-}MeO^-)_2(Cl^-)(MeOH)(H_2O)_{0.5}]$, 6: TBC[4] (100 mg, 0.154 mmol), 2-hydroxyacetophenone oxime (46 mg, 0.308 mmol) and $MnCl_2\cdot 4H_2O$ (183 mg, 0.924 mmol) were dissolved in dmf / MeOH (8mL / 8mL) and the mixture was stirred for 10 minutes. Triethylamine (1.54 mmol, 0.21 mL) was added and the dark brown solution was stirred for an hour before the reaction was filtered. Dark brown crystals of **6**, suitable for single-crystal X-ray diffraction studies, were grown by slow evaporation of the mother liquor. Yield (based on TBC[4]): 45 mg, 22%. $C_{124.5}H_{158}N_{6.5}Mn_8O_{24.5}$: calcd. C 57.24; H 6.10; N 3.48 found C 56.16; H 6.57; N 4.88%. This difference is attributed to solvent loss and disorder within the crystal, precluding accurate calculation of the former. **Crystal data (CCDC 1555665):** $C_{125.5}H_{161.5}ClMn_8N_{6.5}O_{24.5}$, M =2628.07 g/mol, monoclinic, space group $C2/c$ (no. 15), a = 40.676(3) Å, b = 20.8282(13) Å, c = 41.694(3) Å, β = 118.037(2)°, V = 31179(4) Å^3, Z = 8, 122376 reflections measured, 29591 unique (R_{int} = 0.0557) which were used in all calculations. The final R_1 was 0.1027 (I > 2σ(I)) and wR_2 was 0.3360 (all data)

$[Mn^{III}_7Mn^{II}(TBC[4]\text{-}4H)_2(III^{2-})_3(\mu_4\text{-}O^{2-})_2(\mu_3\text{-}O^{2-})(dmf)_3(\mu_2\text{-}MeO^-)_2(NO_3^-)(MeOH)]\cdot 3MeCN$, 7: TBC[4] (100 mg, 0.154 mmol), 2-hydroxypropiophenone oxime (51 mg, 0.308 mmol) and $Mn(NO_3)_2\cdot 4H_2O$ (232 mg, 0.924 mmol) were dissolved in dmf / MeOH (8mL / 8mL) and the mixture was stirred for 10 minutes. Triethylamine (1.54 mmol, 0.21 mL) was added and the dark brown solution was stirred for an additional hour. The reaction mixture was filtered and dark brown crystals of **7**, suitable for single-crystal X-ray diffraction studies, were grown by slow evaporation of the mother liquor. Crystalline samples were contaminated with **III**, precluding calculation of an accurate yield and the study of the magnetic properties. Although this is the case, the structure of **7** has been included here to aid discussion of the steric factors in determining cluster type. **Crystal data (CCDC 1555666):** $C_{134}H_{172.5}Mn_8N_{10.5}O_{26}$, M =2785.83 g/mol, triclinic, space group P-1 (no. 2), a = 15.616(10) Å, b = 19.216(12) Å, c = 25.249(16) Å, α = 104.65(3)°, β = 96.962(17)°, γ = 110.556(13)°, V = 6676(7) Å^3, Z = 4, 99265 reflections measured, 26232 unique (R_{int} = 0.0447) which were used in all calculations. The final R_1 was 0.0648 (I > 2σ(I)) and wR_2 was 0.2006 (all data)

$[Mn^{III}_7Mn^{II}(TBC[4]\text{-}4H)_2(III^{2-})_3(\mu_4\text{-}O^{2-})_2(\mu_3\text{-}O^{2-})(dmf)_2(\mu_2\text{-}MeO^-)_2(Cl^-)(MeOH)_2]\cdot 2MeCN$, 8: TBC[4] (100 mg, 0.154 mmol), 2-hydroxypropiophenone oxime (46 mg, 0.308 mmol) and $MnCl_2\cdot 4H_2O$ (183 mg, 0.924 mmol) were dissolved in dmf / MeOH (8mL / 8mL) and the mixture was stirred for 10 minutes. Triethylamine (1.54 mmol, 0.21 mL) was added and the dark brown solution was stirred for an additional hour. The reaction mixture was filtered and dark brown crystals of **8**, suitable for single-crystal X-ray diffraction stud-

ies, were grown by slow evaporation of the mother liquor. Crystalline samples were contaminated with **III**, precluding calculation of an accurate yield and the study of the magnetic properties. Although this is the case, the structure of **8** has been included here to aid discussion of the steric factors in determining cluster type. **Crystal data (CCDC 1555667):** $C_{129}H_{165}ClMn_8N_7O_{23}$, M =2656.64 g/mol, triclinic, space group P-1 (no. 2), a = 14.04(2) Å, b = 16.52(3) Å, c = 28.99(5) Å, α = 83.39(4)°, β = 76.11(5)°, γ = 75.48(5)°, V = 6308(17) Å^3, Z = 2, 60768 reflections measured, 16823 unique (R_{int} = 0.0810) which were used in all calculations. The final R_1 was 0.0769 (I > 2σ(I)) and wR_2 was 0.2109 (all data)

$[Mn^{IV}_2Mn^{III}_2(X\text{-}2H)_6(X(imine)^{2-})_2]$·dmf·6MeOH, 9: Method (A): TBC[4] (100 mg, 0.154 mmol), 3,5-di-tert-butyl-salicylaldoxime (154 mg, 0.616 mmol) and $Mn(NO_3)_2{\cdot}4H_2O$ (77 mg, 0.308 mmol) were dissolved in a mixture of dmf / MeOH (8mL / 8mL). After stirring for 10 minutes, Et_3N (1.54 mmol, 0.21 mL) was added and the resulting dark green solution was stirred for a further hour. The reaction was filtered and dark green crystals of **9** were grown by slow evaporation of the mother liquor over several days. Method (B) 3,5-di-tert-butyl-salicylaldoxime (100 mg, 0.401 mmol) and $Mn(NO_3)_2{\cdot}4H_2O$ (50 mg, 0.200 mmol) was stirred for 10 minutes in a solution of MeOH (6 mL) and dmf (6 mL). Et_3N (0.07 mL, 0.5 mmol) was added via syringe and the dark green solution was stirred for a further 1 hour. Dark green blocks of **9** were obtained, after several days after slow evaporation of the reaction mixture. Yield (based on 3,5-di-tert-butyl-salicylaldoxime): 52 mg, 40%. $C_{132}H_{208}N_{10}Mn_4O_{22}$: calcd. C 63.24; H 8.05; N 5.59; found C 63.41; H 8.07; N 5.62%. **Crystal data (CCDC 1555668):** $C_{132}H_{208}Mn_4N_{10}O_{22}$, M =2506.84 g/mol, triclinic, space group P-1 (no. 2), a = 15.220(17) Å, b = 15.342(17) Å, c = 19.40(2) Å, α = 66.84(3)°, β = 72.55(2)°, γ = 60.488(14)°, V = 3592(7) Å^3, Z = 1, 51995 reflections measured, 13735 unique (R_{int} = 0.0405) which were used in all calculations. The final R_1 was 0.0651 (>2sigma(I)) and wR_2 was 0.1897 (all data).

ASSOCIATED CONTENT

Supporting Information

The associated Supporting Information includes a table showing structural comparison in the six-atom central belt of **1** – **8**, figures supporting discussion of the magnetic properties of **1** and **3** – **6**, and large versions of Figure 1 and Figures 3 - 8. The Supporting Information is available free of charge on the ACS Publications website (Supporting Information.pdf). CIF Files have been deposited with the Cambridge Structural Database (https://www.ccdc.cam.ac.uk) and can be retrieved using the identifiers listed for each compound.

AUTHOR INFORMATION

Corresponding Author

*E.Brechin@ed.ac.uk
*S.J.Dalgarno@hw.ac.uk

ORCID ID

Euan Brechin: 0000-0002-9365-370X
Scott Dalgarno: 0000-0001-7831-012X

Notes

The authors declare no competing financial interest.

ACKNOWLEDGMENT

We thank EPSRC for financial support of this work through grants EP/H011188 / EP/H011234 and EP/I03255X / EP/I031421.

REFERENCES

(1) (a) Gatteschi, D.; Sessoli, R.; Villain, J. *Molecular Nanomagnets*, Oxford, Oxford University Press, **2006**, and references therein; (b) Wernsdorfer, W.; Sessoli, R. Quantum phase interference and parity effects in magnetic molecular clusters. *Science* **1999**, *284*, 133; (c) Cleuziou, J.-P.; Wernsdorfer, W.; Bouchiat, V.; OndarÅuhu, T.; Monthioux, M. Carbon nanotube superconducting quantum interference device. *Nat. Nanotechnol*., **2006**, *1*, 53; (d) Lehmann, J.; Gaita-Ariño, A.; Coronado, E.; Loss, D. Spin qubits with electrically gated polyoxometalate molecules. *Nat. Nanotechnol*. **2007**, *2*, 312; (e) Baker, M.; Guidi, T.; Carretta, S.; Olivier, J.; Mutka, H.; Gìdel, H.-U.; Timco, G. A.; McInnes, E. J. L.; Amoretti, G.; Winpenny, R. E. P. Spin dynamics of molecular nanomagnets unravelled at atomic scale by four-dimensional inelastic neutron scattering. *Nature Physics* **2012**, *8*, 906; (f) Ganzhorn, M.; Klyatskaya, S.; Ruben, M.; Wernsdorfer, W. Strong spin–phonon coupling between a single-molecule magnet and a carbon nanotube nanoelectromechanical system. *Nat. Nanotechnol*. **2013**, *8*, 165.

(2) (a) Manchanda, R.; Brudvig, G. W.; Crabtree, R. H. High-valent oxomanganese clusters: structural and mechanistic work relevant to the oxygen-evolving center in photosystem II. *Coord. Chem. Rev.* **1995**, *144*, 1; (b) Mukhopadhyay, S.; Mandal, S. K.; Bhaduri, S.; Armstrong, W. H. Manganese Clusters with Relevance to Photosystem II. *Chem. Rev*. **2004**, *104*, 3981.

(3) Lis, T. Preparation, structure, and magnetic properties of a dodecanuclear mixed-valence manganese carboxylate. *Acta Crystallogr.*, **1980**, *B36*, 2042.

(4) Caneschi, A.; Gatteschi, D.; Sessoli, R. Alternating current susceptibility, high field magnetization, and millimeter band EPR evidence for a ground S = 10 state in $[Mn_{12}O_{12}(CH_3COO)_{16}(H_2O)_4].2CH_3COOH.4H_2O$. *J. Am. Chem. Soc*. **1991**, *113*, 5873.

(5) (a) Milios, C. J.; Vinslava, A.; Wood, P. A.; Parsons, S.; Wernsdorfer, W.; Christou, G.; Perlepes, S. P.; Brechin, E. K. A Single-Molecule Magnet with a "Twist". *J. Am. Chem. Soc*. **2007**, *129*, 8; (b) Milios, C. J.; Vinslava, A.; Wernsdorfer, W.; Moggach, S.; Parsons, S.; Perlepes, S. P.; Christou, G.; Brechin, E. K. A Record Anisotropy Barrier for a Single-Molecule Magnet. *J. Am. Chem. Soc*. **2007**, *129*, 2754; (c) Milios, C. J.; Wood, P. A.; Parsons, S.; Foguet-Albiol, D.; Lampropoulous, C.; Christou, G.; Perlepes, S. P.; Brechin, E. K. The use of methylsalicyloxime in manganese chemistry: A $[Mn^{III}_3]$ triangle and its oxidation to a $[Mn^{IV}_4Ce^{III}_2]$ rod. *Inorg. Chim. Acta* **2007**, *360*, 3932; (d) Milios, C. J.; Piligkos, S.; Brechin, E. K. Ground state spin-switching *via* targeted structural distortion: *twisted* single-molecule magnets from derivatised salicylaldoximes. *Dalton Trans*. **2008**, 1809, and references therein.

(6) Gutsche, C. D. Synthesis of Calixarenes and Thiacalixarenes. Chapter 1 in *Calixarenes 2001*, Kluwer Academic Publishers, **2001**, and references therein.

(7) (a) Aronica, C.; Chastanet, G.; Zueva, E.; Borshch, S. A.; Clemente-Juan, J. M.; Luneau, D. A Mixed-Valence Polyoxovanadate(III,IV) Cluster with a Calixarene Cap Exhibiting Ferromagnetic V(III)−V(IV) Interactions. *J. Am. Chem. Soc*. **2008**, *130*, 2365; (b) Karotsis, G.; Teat, S. J.; Wernsdorfer, W.; Piligkos, S.; Dalgarno, S. J.; Brechin, E. K. Calix[4]arene-Based Single-Molecule Magnets. *Angew. Chem. Int. Ed*. **2009**, *48*, 8285; (c) Taylor, S. M.; Karotsis, G.; McIntosh, R. D.; Kennedy, S.; Teat, S. J.; Beavers, C. M.; Wernsdorfer, W.; Piligkos, S.; Dalgarno, S. J.; Brechin, E. K. A Family of Calix[4]arene-Supported $[Mn^{III}_2Mn^{II}_2]$ Clusters. *Chem.-Eur. J*. **2011**, *17*, 7521; (d) Karotsis, G.; Evangelisti, M.; Dalgarno, S. J.; Brechin, E. K. A Calix[4]arene 3d/4f Magnetic Cooler. *Angew. Chem. Int. Ed*. **2009**, *48*, 9928; (e) Karotsis, G.; Kennedy, S.; Teat, S. J.; Beavers, C. M.; Fowler, D. A.; Morales, J. J.; Evangelisti, M.; Dalgarno, S. J.; Brechin, E. K. $[Mn^{III}_4Ln^{III}_4]$ Calix[4]arene Clusters as Enhanced Magnetic Coolers and Molecular Magnets. *J. Am. Chem. Soc*., **2010**, *132*, 12983; (f) Sanz, S.; Ferreira, F.; McIntosh, R. D.; Dalgarno, S. J.; Brechin, E. K. Calix[4]arene-supported $Fe^{III}_2Ln^{III}_2$ clusters. *Chem. Commun*. **2011**, *47*, 9042; (g) Sanz, S.; McIntosh, R. D.; Beavers, C. M.; Teat, S. J.; Evangelisti, M.; Brechin, E. K.; Dalgarno, S. J. Calix[4]arene-supported rare earth octahedra. *Chem. Commun*. **2012**, *48*, 1449; (h) Taylor, S. M.; McIntosh, R. D.; Piligkos, S.; Dalgarno, S. J.; Brechin, E. K. Calixarene-supported clusters: employment of complementary cluster ligands for the construction of a ferromagnetic $[Mn_5]$ cage. *Chem. Commun*. **2012**, *48*, 11190; (i) Palacios, M. A.; McLellan, R.; Beavers, C. M.; Teat, S. J.; Weihe, H.; Piligkos, S.;

Dalgarno, S. J.; Brechin, E. K. Facile Interchange of 3d and 4f Ions in Single-Molecule Magnets: Stepwise Assembly of [Mn_4], [Mn_3Ln] and [Mn_2Ln_2] Cages within Calix[4]arene Scaffolds. *Chem.-Eur. J.* **2015**, *21*, 11212.

(8) McLellan, R.; Taylor, S. M.; McIntosh, R. D.; Brechin, E. K.; Dalgarno, S. J. Complementary ligands direct the formation of a calix[8]arene-supported ferromagnetic $Mn^{IV}Mn^{III}$ dimer. *Dalton Trans.* **2013**, *42*, 6697.

(9) (a) Dunstan, W. R.; Goulding, E. LXXVI.—The action of alkyl haloids on hydroxylamine. Formation of substituted hydroxylamines and oxamines. *J. Chem. Soc., Trans.* **1899**, *75*, 792; (b) Aldred, R.; Johnston, R.; Levin, D.; Neilan, J. Magnesium-mediated ortho-specific formylation and formaldoximation of phenols. *J. Chem. Soc., Perkin Trans.* **1994**, *1*, 1823; (c) Johnson, K.; Degering, E. F. The Utilization of Aliphatic Nitro Compounds. (I) The Production of Amines and (II) The Production of Oximes. *J. Am. Chem. Soc.* **1939**, *61*, 3194.

(10) (a) McLellan, R.; Palacios, M. A.; Beavers, C. M.; Teat, S. J.; Piligkos, S.; Brechin, E. K.; Dalgarno, S. J. Linked Supramolecular Building Blocks for Enhanced Cluster Formation. *Chem.-Eur. J.* **2015**, *21*, 2804; (b) Mukherjee, S.; Abboud, K. A.; Wernsdorfer, W.; Christou, G. Comproportionation Reactions to Manganese(III/IV) Pivalate Clusters: A New Half-Integer Spin Single-Molecule Magnet. *Inorg. Chem.* **2013**, *52*, 873 and references therein; (c) Razali, M. R.; Chesman, A. S. R.; Chilton, N. F.; Langley, S. K.; Moubaraki, B.; Murray, K. S.; Deacon, G. B.; Batten, S. R. Structure and magnetism of a mixed-valence octanuclear manganese(II/III) cluster derived from carbamoylcyanonitrosomethanide (ccnm). *Dalton Trans.* **2013, *42,* 1400**.

(11) Values calculated using Mercury v3.9.

(12) Coletta, M.; McLellan, R.; Murphy, P.; Leube, B. T.; Sanz, S.; Clowes, R.; Gagnon, K. J.; Teat, S. J.; Cooper, A. I.; Paterson, M. J.; Brechin, E. K.; Dalgarno, S. J. Bis-Calix[4]arenes: From Ligand Design to the Directed Assembly of a Metal–Organic Trigonal Antiprism. *Chem.-Eur. J.* **2016**, *22*, 8791; (b) Coletta, M.; McLellan, R.; Cols, J.-M.; Gagnon, K. J.; Teat, S. J.; Brechin, E. K.; Dalgarno, S. J. Investigations into cluster formation with alkyl-tethered bis-calix[4]arenes. *Supramol. Chem.* **2016**, *28*, 557; (c) Coletta, M.; McLellan, R.; Waddington, A.; Sanz, S.; Gagnon, K. J.; Teat, S. J.; Brechin, E. K.; Dalgarno, S. J. Core expansion of bis-calix[4]arene-supported clusters. *Chem. Commun.* **2016**, *52*, 14246.

(13) Stamatatos, T. C.; Christou, G. Mixed valency in polynuclear Mn^{II}/Mn^{III}, Mn^{III}/Mn^{IV} and $Mn^{II}/Mn^{III}/Mn^{IV}$ clusters: a foundation for high-spin molecules and single-molecule magnets. *Philos. Trans. R. Soc.* **2008**, *366*, 113.

(14) Das, A. K.; Peng, S.–M.; Bhattacharya, S. Ruthenium-mediated reduction of oximes to imines. Synthesis, characterization and redox properties of imine complexes of ruthenium. *J. Chem. Soc., Dalton Trans.* **2000**, 181.

(15) (a) Zhou, C.-L.; Wang, Z.-M.; Wang, B.-Wu.; Gao, S. A oximato-bridged linear trinuclear [MnIVMnIIIMnIV] single-molecule magnet. *Dalton Trans.* **2012**, *41*, 13620; (b) Xu, H.-B.; Wang, B.-Wu.; Pan, F.; Wang, Z.-M.; Gao, S. Stringing oxo-centered trinuclear [Mn^{III}_3O] units into single-chain magnets with formate or azide linkers. *Angew. Chem. Int. Ed.*, **2007**, *46*, 7388.

(16) Berg, N.; Rajeshkumar, T.; Taylor, S. M.; Brechin, E. K.; Rajaraman, G.; Jones, L. F. What Controls the Magnetic Interaction in bis-μ-Alkoxo Mn^{III} Dimers? A Combined Experimental and Theoretical Exploration . *Chem.-Eur. J.* **2012**, *18*, 5906.

TOC Graphic

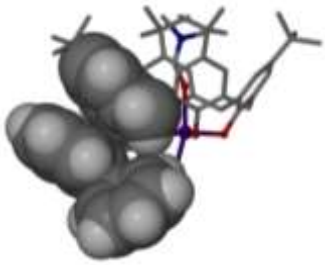

TOC Synopsis

The assembly of multi-component calix[4]arene / salicylaldoxime supported polymetallic clusters is modulated by the steric imposition of a series of substituents on the latter ligand type (complementary interactions between ligands shown in figure). In this way, both structural and magnetic properties of the resultant clusters can be modified, while maintaining the expected coordination chemistry of the respective ligands.